

The Engineer's Guide To EMI In DC-DC Converters (Part 17): Active And Hybrid Filter Circuits

by Timothy Hegarty, Texas Instruments, Phoenix, Ariz.

A compact and efficient design of the electromagnetic interference (EMI) filter is one of the main challenges in high-density dc-dc converter design and is paramount to achieving the full benefits of electrification in automotive, aircraft and shipboard systems, as well as other highly constrained system environments. While differential-mode (DM) and common-mode (CM) passive filters can mitigate conducted EMI generated by a switching power regulator and ensure compliance with conducted EMI standards, practical implementations often occupy more than 30% of the total volume of the power solution. Clearly, minimizing the size, weight and cost of the EMI filter stage remains a priority for system designers.

To this end, there have been numerous efforts over the past three decades in the application of active EMI filters (AEFs), with results indicating a substantial reduction in filter size and volume relative to a passive-only solution. Along with an AEF, the use of another passive component helps improve the overall attenuation and bandwidth—these circuits are known as hybrid EMI filters (HEFs). The design and implementation of AEF and HEF circuits depend on the type of noise (DM or CM) and the required noise-sensing, active-control and noise-cancellation circuits.

This article reviews the theoretical background of AEF circuits in terms of noise sensing, noise injection and control techniques. Experimental results from an automotive synchronous buck regulator circuit—using a novel controller with integrated AEF functionality for DM noise cancellation—illustrate the benefits available to designers in terms of EMI performance and space savings.

An Overview Of Passive And Active Filtering

Passive EMI filtering (PEF) is the intuitive, straightforward and traditional approach to reduce the conducted emissions of a power electronic circuit, even though the size, weight and cost of the passive filter components cause significant constraints in some applications. As detailed in parts 15 and 16 of this article series,^[1-16] passive filter design relies on the insertion of high-impedance series elements (inductors, ferrite beads, CM chokes) and low-impedance shunt elements (capacitors) to create an impedance mismatch in the EMI current path. The low-order switching harmonics usually dictate the size of the passive filter components.

In contrast, an AEF circuit^[17-25] uses active devices and control to sense the residual disturbance and inject an opposing disturbance that directly attenuates the EMI current measured at the input. Based on the superposition theorem of signals with equal amplitude and opposite phase, the injected voltage or current should theoretically cancel or nullify the incident input ripple voltage or current contribution from the EMI source. The expectation is that AEF reduces EMI and results in a smaller-size filter compared to an equivalent passive design.

As an introduction, let's look at the simplified passive and active filter circuits in Fig. 1 specifically for DM noise attenuation, where $i_S(s)$ and $Z_S(s)$ designate the Norton-equivalent noise current source and parallel source impedance of the power stage.

The active EMI filter configured with voltage sense and current injection in Fig. 1b uses an operational amplifier (op amp) stage as a capacitive multiplier to effectively replace filter capacitor C_F in the passive design and support a lower value for filter inductor L_F . Fig. 1 includes expressions for the filter cutoff frequencies.

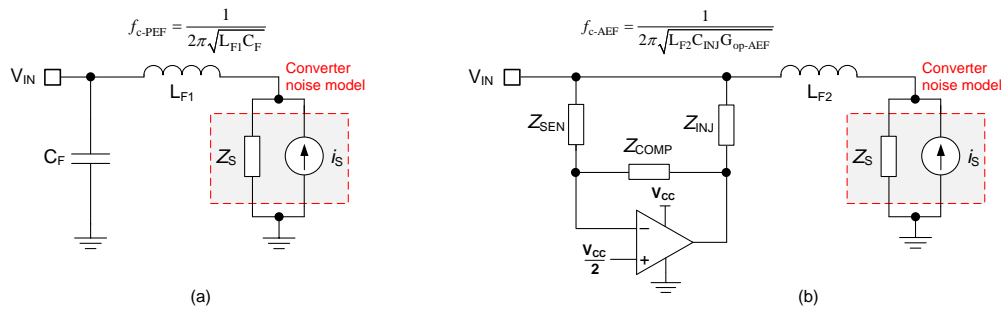


Fig. 1. Simplified passive filter (a) and hybrid active filter (b) for DM noise attenuation, along with the converter DM noise model using a Norton-equivalent representation.

Depending on the gain and bandwidth of the active circuit, AEF enables attenuation at the fundamental switching frequency and low-order harmonics, while relatively small-sized passive components (with lower parasitic contributions) provide supplementary attenuation at higher frequencies where the gain of the active stage rolls off. The passive component volume reduction directly relates to the attenuation provided by the AEF.^[20]

AEF Circuit Configurations

Fig. 2 illustrates six active-filter topologies classified according to the sensed noise parameter, the means by which the cancellation signal is injected, and the active control technique, as follows:

- Voltage sense (VS) or current sense (CS)
- Voltage injection (VI) or current injection (CI)
- Feedback (FB) control or a feedforward (FF) control structure.

Such classification generally applies to both the DM and CM functional units of the overall filter in dc-dc (as well as ac-dc) systems.

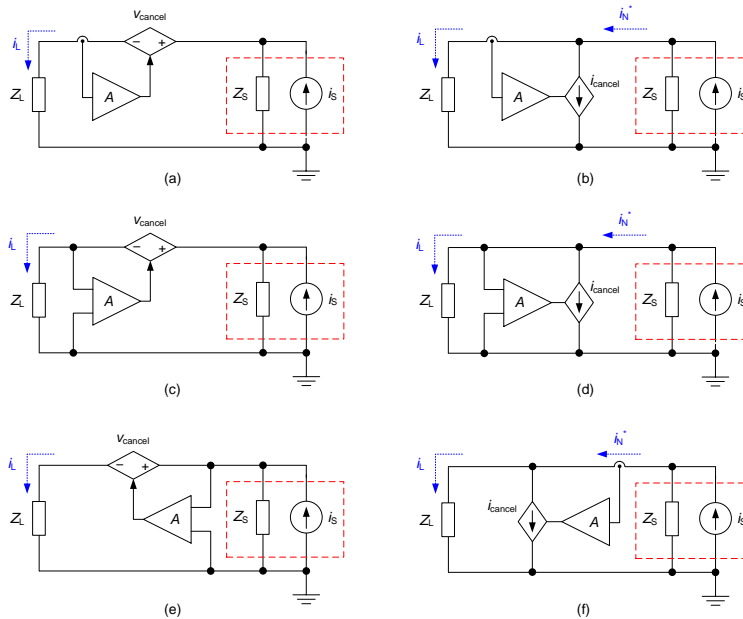


Fig. 2. Active filter topologies (four FB circuits and two FF designs) categorized according to their control, sensing and injection techniques: FB-CSVI (a), FB-CSCI (b), FB-VSVI (c), FB-VSCI (d), FF-VSVI (e) and FF-CSCI (f).

In Fig. 2, Z_s is the Norton noise source impedance, Z_L is the impedance at the noise receiving end (for example, the line impedance stability network (LISN) for EMI measurement) and A represents the gain of the active circuit. Adding different passive elements in place of Z_s and Z_L will form different HEF circuits.

In terms of noise cancellation, VI designs use a controlled *series* voltage source to impede the flow of the noise current to the LISN, whereas CI designs involve a controlled *shunt* current source to reroute the flow of the noise current produced by the noise source.

From a control standpoint, FB designs sense the residual disturbances at the load or LISN side, and inject (with high gain) a cancellation signal back into the system at the source side. FF circuits measure the disturbance close to the noise source and inject (with unity gain) a cancellation signal on the load side.^[20] Table 1 summarizes the salient characteristics of the AEF circuits embodied in Fig. 2.

Table 1. AEF circuits from Fig. 2 categorized by control, sensing and injection techniques.

| AEF topology | | Control | Sensing | Injection | Active element for injection |
|--------------|---------|-------------|---------|-----------|-----------------------------------|
| a | FB-CSVI | Feedback | Current | Voltage | Current-controlled voltage source |
| b | FB-CSCI | Feedback | Current | Current | Current-controlled current source |
| c | FB-VSVI | Feedback | Voltage | Voltage | Voltage-controlled voltage source |
| d | FB-VSCI | Feedback | Voltage | Current | Voltage-controlled current source |
| e | FF-VSVI | Feedforward | Voltage | Voltage | Voltage-controlled voltage source |
| f | FF-CSCI | Feedforward | Current | Current | Current-controlled current source |

Because magnetic components for current sensing and voltage injection are generally large and may not result in an overall volume reduction, it is better to select an AEF topology that precludes the use of additional magnetic components. The VSCI topology uses capacitors (rated for the input voltage) in combination with low-voltage active circuits (powered from a bias supply of 5 V) for noise sensing and injection.

Circuit Simulation

Fig. 3 shows a simulation model of a synchronous buck regulator with an FB-VSCI DM AEF circuit, providing an output of 5 V and 10 A from an automotive battery input of 13.5 V. The switching frequency is 440 kHz.

Fig. 4 provides the simulated waveforms, including AEF amplifier output voltage and current, power-stage input voltage and current, and LISN output voltage. Fig. 3 does not include modeled CM noise currents, so the DM model of the LISN output provides the DM noise signature.

The amplifier sources and sinks approximately 45 mA such that the AEF circuit effectively shunts the ripple current from the input filter inductor L_F to ground.

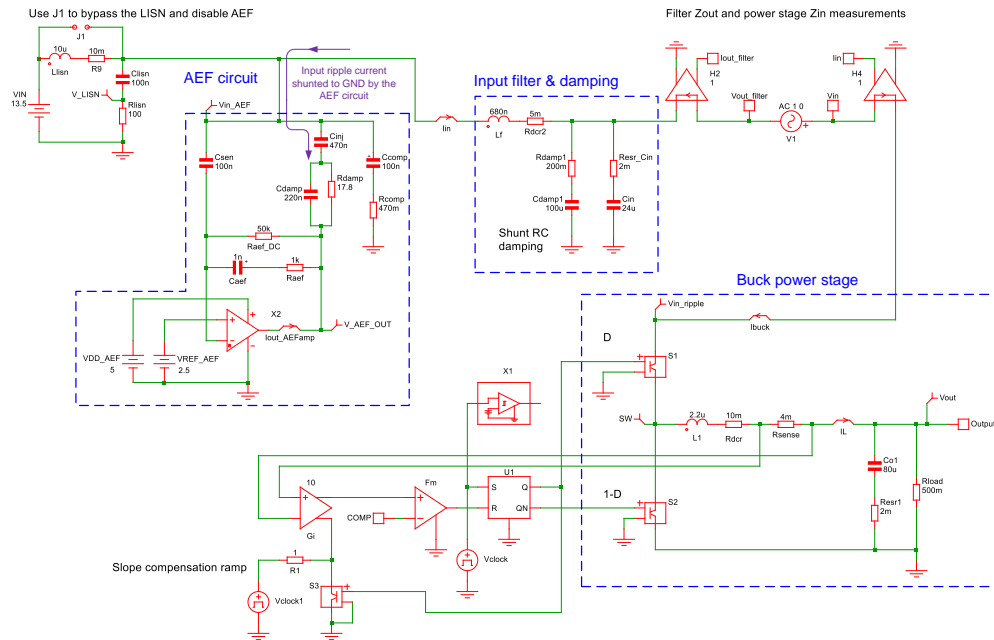


Fig. 3. Simulation model of a buck regulator with the preferred hybrid FB-VSCI AEF topology.

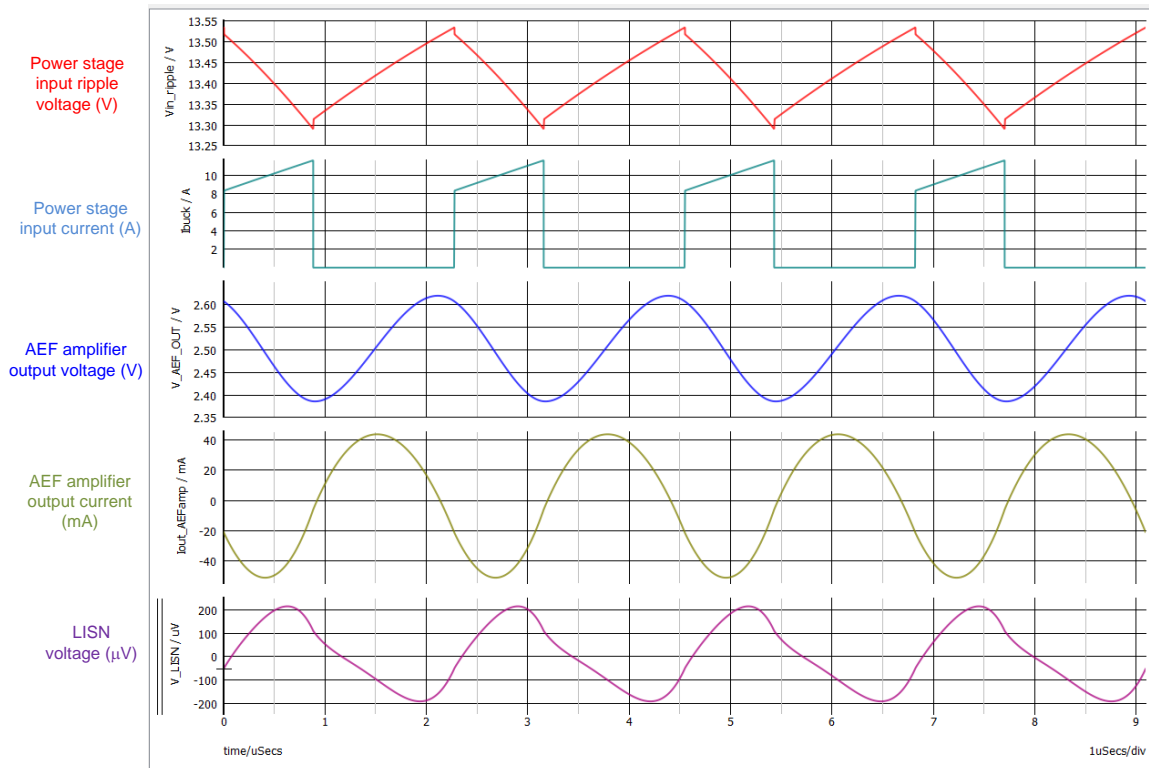


Fig. 4. AEF simulated waveforms.

AEF Circuit Design

AEF Components

The active filter sensing, injection and compensation networks shown in Fig. 3 use relatively low capacitance values (with small component footprints) to design a gain term denoted as G_{op-AEF} . The effective active capacitance is set by the product of G_{op-AEF} and the injection capacitance C_{INJ} . The effective gain G_{op-AEF} enables an active design with reduced inductor and capacitor values and a filter cutoff frequency equivalent to that of the passive implementation (see Fig. 1). Equation 1 gives the equivalent impedance of the AEF as:

$$Z_{eq}(s) = \frac{Z_{out-op}(s) + Z_{inj}(s)}{1 + G_{op-AEF}(s)} \quad (1)$$

where Z_{out-op} is the open-loop output impedance of the op amp, G_{op-AEF} is the voltage gain from the sensed noise voltage to the amplifier output voltage and Z_{inj} is the impedance of the injection network.

AEF Loading

Any capacitive loading of the AEF amplifier reduces the phase margin of the active circuit. In an AEF application, the input capacitance of the converter would effectively form a very large capacitive load to the op amp. An inductance is therefore required between the input capacitors and the AEF circuit to prevent the active circuit from being loaded by the input capacitance. This decoupling inductance can be a discrete inductor, a ferrite bead or the leakage inductance of a CM choke. In Fig. 3, L_F serves this purpose.

Based on the trapezoidal current of the high-side switch feeding a low equivalent series resistance (ESR) ceramic-input capacitance, the power-stage input voltage ripple is effectively a triangular waveform. By deriving the volt-seconds across inductor L_F , equation 2 gives a convenient expression for the $L_F C_{IN}$ product to set up a specified peak-to-peak (sinusoidal) ripple current in L_F within the sink and source current capability of the AEF amplifier:

$$L_F C_{IN} = \frac{D(1-D)I_{OUT}}{8I_{Lpk-pk}F_{sw}^2} \quad (2)$$

where I_{Lpk-pk} is the peak-to-peak ripple current in L_F , which is highest when duty cycle D is 50%.

The inductor ripple current effectively flows through the injection capacitor and should be within the sink and source capability of the op amp (with some margin allocated for transients and low-frequency disturbances). It is possible to optimize both L_F and C_{IN} to achieve the appropriate ripple current amplitude. A lower C_{IN} value also has the benefit of reducing the bulk damping capacitance, normally set to four times C_{IN} .^[10]

AEF Small-Signal Stability

The op amp in the above example has an open-loop gain of 65 dB and a unity-gain bandwidth of 300 MHz to enable high noise attenuation. While the FB topology is resilient to component tolerances, it is subject to stability issues at low (under 150 kHz) and high (above 10 MHz) frequencies.

Low-frequency instability may occur due to resonance between the capacitive AEF circuit and the inductor that forms the hybrid filter. For a high-gain AEF, the dominant pole of the op amp used in the active circuit can reduce the phase margin. Furthermore, high-frequency instability can occur because of various parasitic components and a second pole of the op amp present in the AEF. Therefore, stability analysis is essential to derive suitable compensation techniques for the AEF.^[26-27]

In Fig. 3, C_{SEN} and C_{INJ} are the sensing and injection capacitors; R_{DAMP} and C_{DAMP} provide parallel damping; R_{DC-AEF} provides dc feedback to bias the output of the op amp; and R_{C1-AEF} , C_{C1-AEF} , R_{C2-AEF} and C_{C2-AEF} ensure low- and high-frequency system stability. Equation 3 provides expressions^[26] to calculate the damping components:

$$R_{DAMP} = \sqrt{\frac{G_{op-AEF} L_F}{C_{INJ}}}, \quad G_{op-AEF} \approx \frac{C_{SEN}}{C_{C1-AEF}}, \quad C_{DAMP} = \frac{C_{INJ}}{2} \quad (3)$$

Practical Implementation

Fig. 5 presents a full schematic of the LM25149-Q1, a synchronous buck dc-dc controller with integrated AEF^[26] from Texas Instruments (TI). This design has the same operating conditions and component values as embodied in Fig. 3.

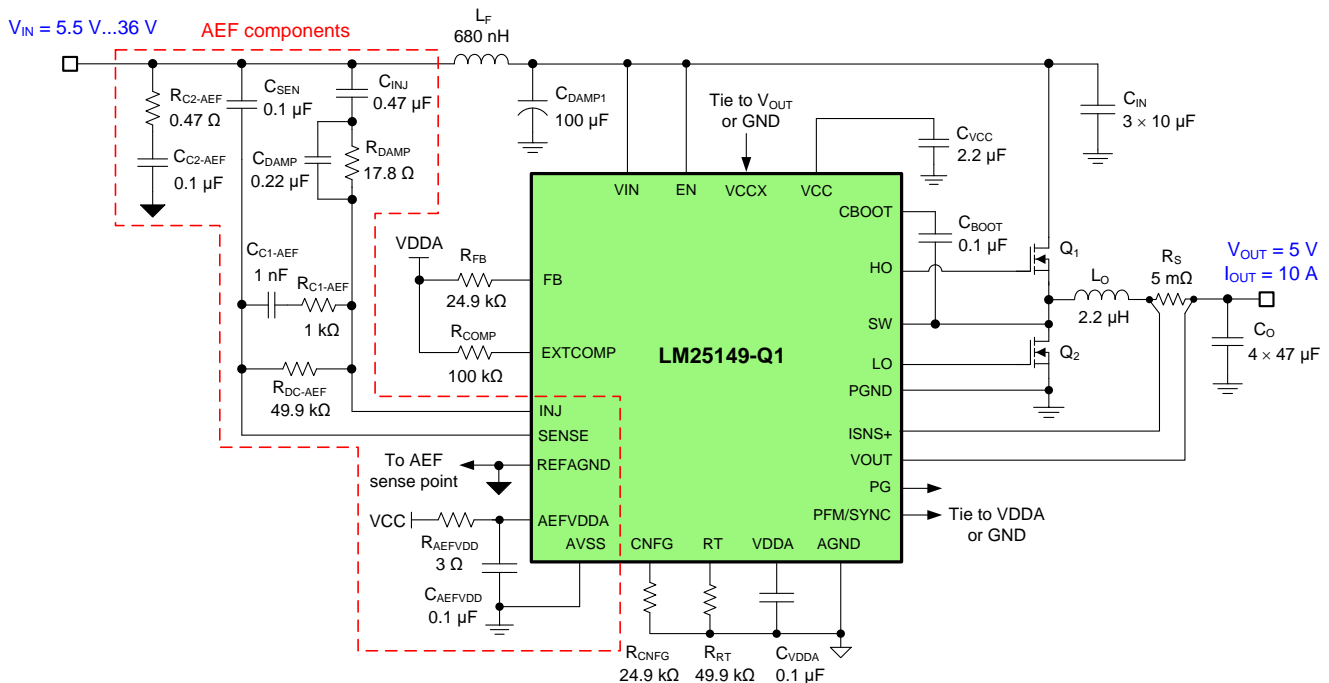


Fig. 5. Schematic of a synchronous buck controller design with integrated AEF.

Separate ground pins for the AEF amplifier supply and its reference, designated as AVSS and REFAGND in Fig. 5, reduce near-field mutual coupling from the switching circuits of the controller. REFAGND is Kelvin-connected to the sense location on the board to obtain differential sensing of the input noise voltage. The AEF circuit derives power from AEFVDDA through an RC filter from the main VCC rail.

Using this hardware platform, Fig. 6 compares passive and active EMI filter designs based on conducted EMI tests to meet the strictest limit (Class 5) of the CISPR 25 automotive standard. The filter component values are captioned in each plot, and the nameplate ceramic capacitance values are subject to derating for applied voltage. The input voltage is 13.5 V.

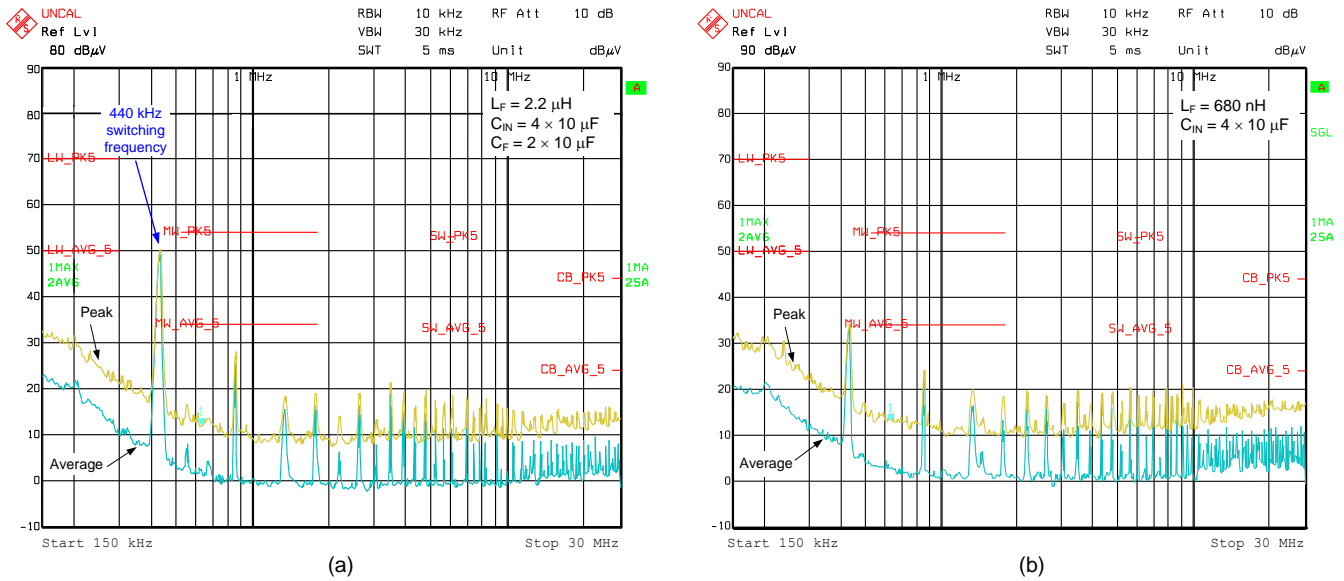


Fig. 6. Comparison of EMI results with a passive filter solution (a) and active filter design (b) given equivalent power-stage operating conditions.

Fig. 7 presents the EMI results when the AEF circuit shown in Fig. 5 is enabled and disabled. Noise cancellation with AEF shows how much better low- and medium-frequency attenuation is relative to a design with AEF switched off. The fundamental frequency component at 440 kHz has its peak EMI level reduced by 50 dB, making it much easier for designers to meet strict EMI requirements.

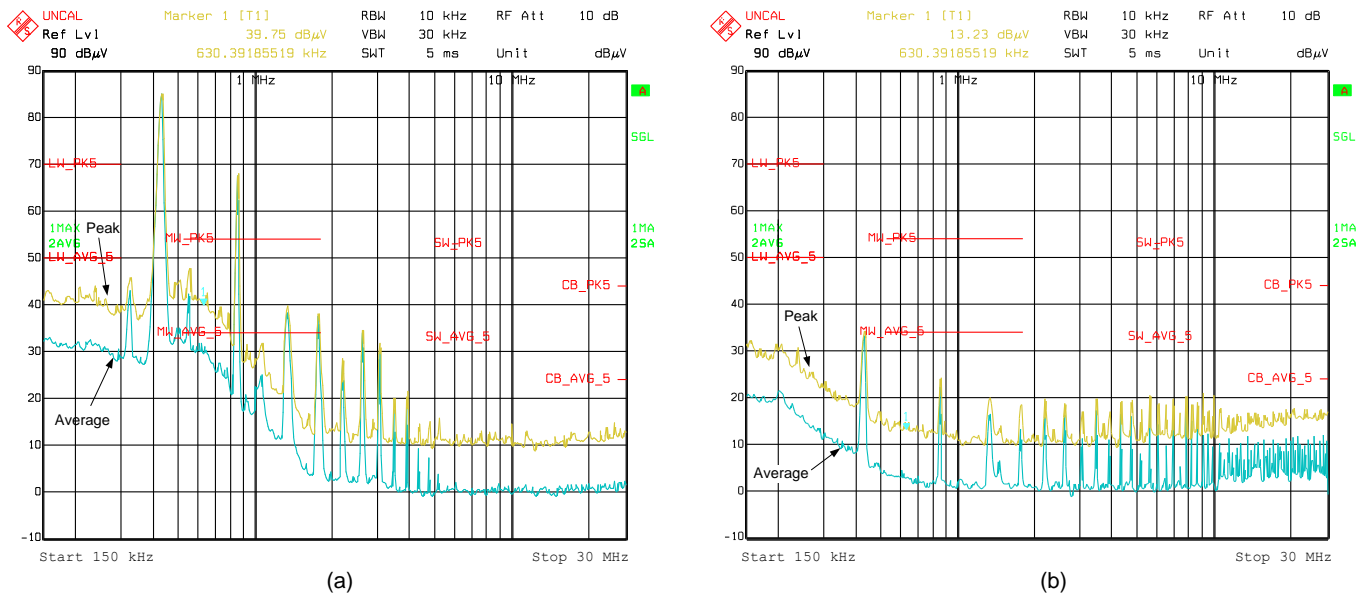


Fig. 7. Comparison of circuit performance when AEF is disabled (a) and enabled (b).

Fig. 8 offers a printed circuit board (PCB) layout comparison of the passive and active filter stages that provided the results in Fig. 6. The filter inductor footprint reduces from 5 mm by 5 mm to 4 mm by 4 mm. Moreover, a physically smaller inductor typically has a winding geometry with a lower parasitic winding capacitance and higher self-resonant frequency, leading to better filtering performance in the higher conducted-frequency range

for CISPR 25: 30 MHz to 108 MHz. Furthermore, several small 0402 or 0603 components for AEF sensing, injection, damping and compensation replace two 1210 capacitors that derate significantly with applied voltage. The footprint and volume of the filter solution decrease by nearly 50% and over 75%, respectively.

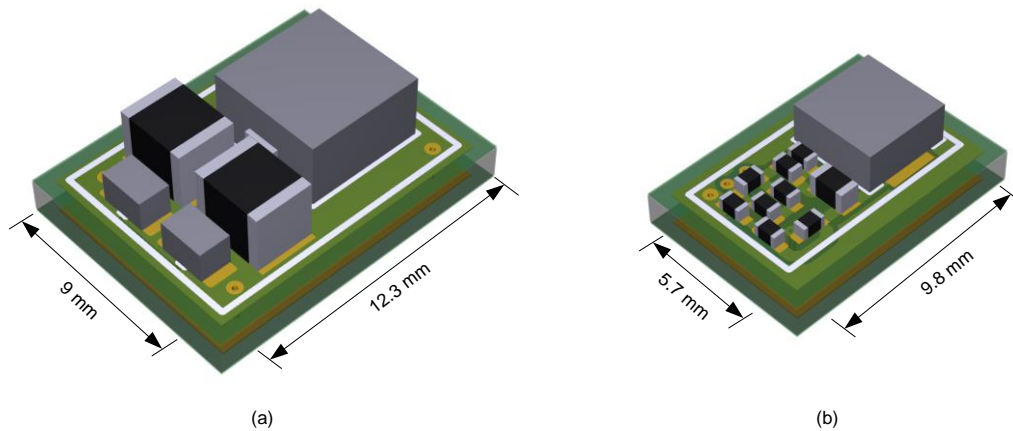


Fig. 8. PCB layout size comparison of passive (a) and active (b) filter designs with equivalent low-frequency attenuation performance.

Summary

Trends in power electronics toward smaller packaging, higher densities, improved performance, reduced weight and lower cost necessitate a reconsideration of EMI filter design. Within this context, a compact and efficient design for the EMI filter stage is one of the critical challenges in high-density dc-dc converter design, particularly for automotive applications. This article presented an introduction to active filtering and an example of a buck controller design with integrated AEF functionality for DM noise cancellation.

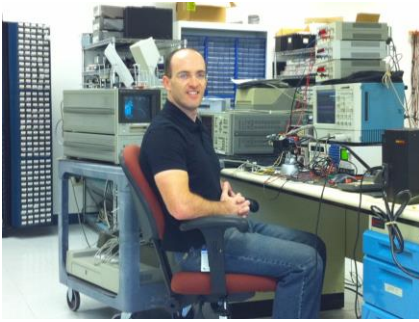
Experimental results indicated a reduction of filter size and volume, enabling high-density filter solutions for next-generation power solutions. The AEF provides attenuation up to approximately 5 MHz, depending on the bandwidth of the circuit, while relatively small passive components (with low parasitics) realize the remaining attenuation requirement in the high-frequency range.

References

1. [“The Engineer’s Guide To EMI In DC-DC Converters \(Part 1\): Standards Requirements And Measurement Techniques”](#) by Timothy Hegarty, How2Power Today, December 2017 issue.
2. [“The Engineer’s Guide To EMI In DC-DC Converters \(Part 2\): Noise Propagation And Filtering”](#) by Timothy Hegarty, How2Power Today, January 2018 issue.
3. [“The Engineer’s Guide To EMI In DC-DC Converters \(Part 3\): Understanding Power Stage Parasitics”](#) by Timothy Hegarty, How2Power Today, March 2018 issue.
4. [“The Engineer’s Guide To EMI in DC-DC Converters \(Part 4\): Radiated Emissions”](#) by Timothy Hegarty, How2Power Today, April 2018 issue.
5. [“The Engineer’s Guide To EMI In DC-DC Converters \(Part 5\): Mitigation Techniques Using Integrated FET Designs”](#) by Timothy Hegarty, How2Power Today, June 2018 issue.
6. [“The Engineer’s Guide To EMI In DC-DC Converters \(Part 6\): Mitigation Techniques Using Discrete FET Designs”](#) by Timothy Hegarty, How2Power Today, September 2018 issue.
7. [“The Engineer’s Guide To EMI In DC-DC Converters \(Part 7\): Common-Mode Noise Of A Flyback”](#) by Timothy Hegarty, How2Power Today, December 2018 issue.
8. [“The Engineer’s Guide To EMI In DC-DC Converters \(Part 8\): Common-Mode Noise Mitigation In Isolated Designs”](#) by Timothy Hegarty, How2Power Today, February 2019 issue.

9. "[The Engineer's Guide To EMI In DC-DC Converters \(Part 9\): Spread-Spectrum Modulation](#)" by Timothy Hegarty, How2Power Today, August 2019 issue.
10. "[The Engineer's Guide To EMI In DC-DC Converters \(Part 10\): Input Filter Impact On Stability](#)" by Timothy Hegarty, How2Power Today, November 2019 issue.
11. "[The Engineer's Guide To EMI In DC-DC Converters \(Part 11\): Input Filter Impact On Dynamic Performance](#)" by Timothy Hegarty, How2Power Today, January 2020 issue.
12. "[The Engineer's Guide To EMI In DC-DC Converters \(Part 12\): Predicting The Differential-Mode Conducted Noise Spectrum](#)" by Timothy Hegarty, How2Power Today, April 2020 issue.
13. "[The Engineer's Guide To EMI In DC-DC Converters \(Part 13\): Predicting The Common-Mode Conducted Noise Spectrum](#)" by Timothy Hegarty, How2Power Today, June 2020 issue.
14. "[The Engineer's Guide To EMI In DC-DC Converters \(Part 14\): Behavioral Noise Modeling](#)" by Timothy Hegarty, How2Power Today, August 2020 issue.
15. "[The Engineer's Guide To EMI In DC-DC Converters \(Part 15\): Differential-Mode Input Filter Design](#)," by Timothy Hegarty, How2Power Today, October 2020 issue.
16. "[The Engineer's Guide To EMI In DC-DC Converters \(Part 16\): Common-Mode Input Filter Design](#)," by Timothy Hegarty, How2Power Today, December 2020 issue.
17. "[Time-saving and cost-effective innovations for EMI reduction in power supplies](#)" by Yogesh Ramadass et al., TI white paper, literature No. SLYY200, March 2021.
18. "[How to reduce EMI and shrink power-supply size with an integrated active EMI filter](#)," by Orlando Murray, TI technical article, April 2021.
19. "[Introduction of active filters for EMI mitigation in DC/DC converters: passive and active EMI filtering methods](#)" by Djilali Hamza, Lambert Academic Publishing, August 2009.
20. "[A survey of active EMI filters for conducted EMI noise reduction in power electronic converters](#)" by Balaji Narayanasamy and Fang Luo, *IEEE Transactions on Electromagnetic Compatibility*, Vol. 61, No. 6, December 2019, pp. 2040-2049.
21. "[Generalization of active filters for EMI reduction and harmonics compensation](#)" by Yo-Chan Son and Seung-Ki Sul, *IEEE Transactions on Industry Applications*, Vol. 42, No. 2, March-April 2006, pp. 545-551.
22. "[Modeling and stability analysis of active/hybrid common-mode EMI Filters for DC/DC power converters](#)" by Yongbin Chu et al., *IEEE Transactions on Power Electronics*, Vol. 31, No. 9, September 2016, pp. 6254-6263.
23. "[Design of a wide bandwidth active filter for common mode EMI suppression in automotive systems](#)" by Alessandro Amaducci, *IEEE International Symposium on Electromagnetic Compatibility & Signal/Power Integrity (EMCSI)*, August 2017, pp. 612-618.
24. "[High density EMI mitigation solution using active approaches](#)" by Balaji Narayanasamy et al., 2017 EMCSI, August 2017, pp. 813-818.
25. "[Design of an active differential mode current filter for a boost power factor correction AC-DC converter](#)" by Rajib Goswami et al., *IEEE Energy Conversion Congress and Exposition*, September 2015, pp. 4375-4382.
26. "[Optimal damping of EMI filter input impedance](#)" by Lei Xing et al., *IEEE Transactions on Industry Applications*, Vol. 47, No. 3, May-June 2011, pp. 1432-1440.
27. "[LM25149-Q1](#) 42-V automotive synchronous buck DC/DC controller with ultra-low I_q and integrated active EMI filter," TI data sheet, April 2021.

About The Author



Timothy Hegarty is a senior member of technical staff (SMTS) in the Buck Switching Regulators business unit at Texas Instruments. With over 23 years of power management engineering experience, he has written numerous conference papers, articles, seminars, white papers, application notes and blogs.

Tim's current focus is on enabling technologies for high-frequency, low-EMI, isolated and nonisolated regulators with wide input voltage range, targeting industrial, communications and automotive applications in particular. He is a senior member of the IEEE and a member of the IEEE Power Electronics, Industrial Applications and EMC Societies.

For more information on EMI, see How2Power's [Power Supply EMI Anthology](#). Also see the How2Power's [Design Guide](#), locate the Design Area category and select "EMI and EMC".